Ion permeation properties of the glutamate receptor channel in cultured embryonic *Drosophila* myotubes

Hangil Chang, Sergio Ciani and Yoshiaki Kidokoro*

Department of Physiology, Jerry Lewis Neuromuscular Research Center and Brain Research Institute, University of California at Los Angeles, Los Angeles, CA 90024, USA

1. Ion permeation properties of the glutamate receptor channel in cultured myotubes of *Drosophila* embryos were studied using the inside-out configuration of the patch-clamp technique.

2. Lowering the NaCl concentration in the bath (intracellular solution), while maintaining that of the external solution constant, caused a shift of the reversal potential in the positive direction, thus indicating a higher permeability of the channel to Na^+ than to Cl^- ($P_{Cl}/P_{Na} < 0{\cdot}04$), and suggesting that the channel is cation selective.

3. With 145 mM Na^+ on both sides of the membrane, the single-channel current–voltage relation was almost linear in the voltage range between −80 and +80 mV, the conductance showing some variability in the range between 140 and 170 pS.

4. All monovalent alkali cations tested, as well as NH_4^+, permeated the channel effectively. Using the Goldman–Hodgkin–Katz equation for the reversal potential, the permeability ratios with respect to Na^+ were estimated to be: 1·32 for K^+, 1·18 for NH_4^+, 1·15 for Rb^+, 1·09 for Cs^+, and 0·57 for Li^+.

5. Divalent cations, i.e. Mg^{2+} and Ca^{2+}, in the external solution depressed not only the inward but also the outward Na^+ currents, although reversal potential measurements indicated that both ions have considerably higher permeabilities than Na^+ ($P_{Mg}/P_{Na} = 2{\cdot}31$; $P_{Ca}/P_{Na} = 9{\cdot}55$).

6. The conductance–activity relation for Na^+ was described by a hyperbolic curve. The maximal conductance was about 195 pS and the half-saturating activity 45 mM. This result suggests that Na^+ ions bind to sites in the channel.

7. All data were fitted by a model based on the Eyring's reaction rate theory, in which the receptor channel is a one-ion pore with three energy barriers and two internal sites.

L-Glutamate is one of the most important excitatory transmitters in the mammalian central nervous system, where it activates a variety of pharmacologically and electrophysiologically distinct receptors (Foster & Fagg, 1984; Mayer & Westbrook, 1987*a*; Monaghan, Bridges & Cotman, 1989; Collingridge & Lester, 1989). In arthropods, including *Drosophila*, L-glutamate is known to be the transmitter at the neuromuscular junction (Takeuchi & Takeuchi, 1964; Usherwood & Cull-Candy, 1975; Jan & Jan, 1976*a*, *b*; Ikeda, 1980). Interest in the insect glutamate receptor has recently been enhanced by the successful cloning of its subunit cDNA (Schuster, Ultsch, Schloss, Cox, Schmitt & Betz, 1991). We have previously investigated the gating kinetics of the channel in embryonic *Drosophila* myotubes (Kidokoro & Chang, 1991), demonstrating that the channel opens in two modes, brief and long bursts, and that binding of two glutamate molecules is required to activate the channel to its main long open state. In this study, we have characterized its ion permeation properties.

Since Na^+ is probably the major charge carrier through the glutamate receptor channel in physiological conditions, we examined extensively the single-channel current–voltage (I–V) behaviour in the presence of Na^+. Moreover, in view of the importance of Ca^{2+} and Mg^{2+} as modulators and blockers of certain types of glutamate receptor channels (Nowak, Bregestovski, Ascher, Herbet & Prochiantz, 1984; Mayer, Westbrook & Guthrie, 1984; Mayer & Westbrook, 1987*b*; Ascher & Nowak, 1988; Iino, Ozawa & Tsuzuki, 1990), we also studied the effects of these divalent ions on the single-channel current.

The single-channel current–voltage (I–V) relations under various ionic conditions were satisfactorily fitted by a three-barrier, two-site Eyring model, assuming single-ion occupancy of the channel.

*To whom correspondence should be addressed at: Gunma University School of Medicine, 3-39-22 Showa-machi, Maebashi, Gunma 371, Japan.

METHODS

Cell cultures

Primary cultures of embryonic *Drosophila* myotubes were prepared as described previously (Kidokoro & Chang, 1991). Briefly, wild-type embryos (Oregon-R) were incubated for 6–8 h at room temperature (22 °C) after fertilization. After dechorionation, cells were transferred into a drop of culture medium on the glass surface. Schneider's *Drosophila* medium with reduced glutamate concentration (100 μM, instead of 4·7 mM) was prepared, to avoid possible effects of high concentrations of the transmitter on glutamate receptor channels during culture. Culture medium was supplemented with 20 % (v/v) fetal calf serum, 50 units ml^{-1} penicillin G sodium, and 50 mg ml^{-1} streptomycin sulphate. Cultures were incubated at 25 °C in humidified air for 14–24 h prior to experiments.

Solutions

The compositions of the solutions are listed in Table 1. Solution A is the standard extracellular (pipette) solution. Solution B is the standard intracellular (bath) solution. A high concentration of L-glutamate (10 mM) was necessary to obtain a frequent occurrence of long (> 10 ms) opening events (Kidokoro & Chang, 1991). For measurement of the reversal potential with various intracellular NaCl concentrations, NaCl in the standard intracellular solution was replaced isosmotically with sucrose by mixing solutions B and C. Sucrose was chosen because our preliminary experiments showed that all large monovalent cations tested (*N*-methyl-D-glucamine, tris(hydroxymethyl)aminomethane (Tris), and arginine) blocked the current carried by Na^+ in a similar manner to the case of the ACh receptor channel (Lewis, 1979; Sanchez, Dani, Siemen & Hille, 1986). In experiments with various monovalent cations, solution D was used as the extracellular solution. In experiments with divalent cations, the desired composition was achieved by mixing solutions A and E (for Mg^{2+}), or solutions A and F (for Ca^{2+}). For studying the effect of Na^+ on the conductance, the NaCl concentrations on both sides of the patch membrane were reduced symmetrically and isosmotically, by mixing solutions G and I (for the extracellular solution), or solutions H and J (for the intracellular one).

In each solution, the amount of NaOH required to titrate the solution to pH 7·1 was measured and taken into account for a correct estimate of the total concentration of Na^+.

Stocks of 1 M monosodium L-glutamate dissolved in distilled water were stored frozen and were freshly thawed for use on each day of the experiments.

Amino acids for use in culture medium were purchased from Sigma (St Louis, MO, USA). Other reagents for culture were obtained from Gibco (Grand Island, NY, USA).

Junction potentials were measured for each pair of intracellular and extracellular solutions. The largest junction potential (5·1 mV, relative to bath) was obtained between 17·5 mM NaCl (bath) and 140 mM NaCl (pipette) solutions, and other junctional potentials were in the range between −3 and +3 mV. The membrane potentials were calculated as a sum of the pipette holding potential and the junction potential.

Recording

Using the conventional patch-clamp technique in the inside-out patch configuration (Hamill, Marty, Neher, Sakmann & Sigworth, 1981), the currents were recorded with an Axopatch 1B amplifier (Axon Instruments, Burlingame, CA, USA). The pipettes, fabricated from soft glass capillaries (micropipettes 75 μl, Drummond Sci. Co., Broomall, PA, USA), were coated with Sylgard (Dow Corning Corp., Midland, MI, USA) and fire-polished shortly before use. Their resistance was 1–5 MΩ when filled with the standard external solution. Just before contacting the cell, the pipette potential was adjusted to the bath reference potential. After forming a gigaseal, an inside-out patch was obtained by quickly withdrawing the pipette from the cell. Sometimes, when the excised patch formed a vesicle, it was necessary to lift the pipette tip briefly out of the solution.

Data acquisition and control of the pipette potential were done using a LabMaster A–D and D–A converter (Scientific Solutions, Solon, OH, USA), connected to an IBM PC-AT compatible computer. Currents were low-pass filtered at 1 or 5 kHz (4-pole Bessel, −3 dB) and directly digitized at a 50 kHz sampling rate and 0·05 pA resolution. As the frequency of the channel openings was usually low (< 0·1 events s^{-1}), the following sampling protocol was used. The sampling program monitored the digitized data and stored them in a circular memory buffer (512 data points, or 10·24 ms at a sampling rate of 50 kHz), until the data crossed a pre-set threshold, which was fixed at the mid-point between the closed and the open state. After threshold crossing, the data were stored in the main buffer (32000 data points, or 640 ms) and sampling was continued until the current level remained under the

Table 1. Composition of solutions

	NaCl	KCl	XCl*	$MgCl_2$	$CaCl_2$	Sodium-L-glutamate	Sucrose	Hepes
A	130	5	0	0	0	10	0	5
B	140	5	0	0	0	0	0	5
C	0	5	0	0	0	0	280	5
D	0	0	135	0	0	10	0	5
E	0	0	0	90	0	10	0	5
F	0	0	0	0	90	10	0	5
G	145	0	0	0	0	1	0	2
H	146	0	0	0	0	0	0	2
I	0	0	0	0	0	1	290	2
J	1	0	0	0	0	0	290	2

*X represents Li^+, K^+, Rb^+, Cs^+ or NH_4^+. All concentrations are in mM. The solutions were buffered with Hepes and adjusted to pH 7·1 with NaOH. Osmolality of the solutions was approximately 295 mosmol kg^{-1}.

threshold for 512 consecutive data points. The current trace was reconstructed from the circular and the main buffer, so that for each opening event both the preceding and the trailing 10·24 ms of the 'closed-state' current level were recorded. Usually, one to ten opening events were collected for each holding potential. The sampled data were finally stored on floppy disks and optical disks for off-line analysis.

All experiments were done at room temperature (21–23 °C).

Analyses

Each channel event record was redrawn on the computer display and visually checked. Open events which had a clear rectangular shape were selected for analysis. In these long events we were able to measure the open channel level without problems due to the limited frequency response of the recording system. The single-channel current amplitude was calculated as the difference between the baseline and open channel level, both of which were determined by manually adjusting the cursors on the display. The reversal potential was determined from the crossing point of the linear interpolation of the I–V relation with the voltage axis. In every case, the membrane potential was changed by a sufficiently large amount to reverse the sign of the single-channel current. The relative permeability, P_X/P_{Na}, of cation X with respect to Na^+ was calculated using the Goldman–Hodgkin–Katz (GHK) equation (Goldman, 1943; Hodgkin & Katz, 1949):

$$I = \frac{z^2PF^2V}{RT}\left(\frac{[X]_i - [X]_o \exp(-zFV/RT)}{1-\exp(-zFV/RT)}\right), \quad (1)$$

The subscripts 'i' and 'o' denote internal and external ion species, respectively. P is the permeability of the ion, V is the membrane potential, z is the valency of the ion, and F, R and T have their usual meanings. The current carried by each ion was calculated from eqn (1). In order to evaluate the permeability ratio P_X/P_{Na}, the sum of the partial currents corresponding to the cations present was set to zero, and the equation was solved for P_X/P_{Na}. Currents carried by anions were neglected in the equation, because, as described in the Results section, P_{Cl}/P_{Na} was found to be low ($< 0{\cdot}04$). Equations (2), (3) and (4) were derived for each type of the following experimental solutions: (a) solutions containing only Na^+ and K^+; (b) solutions containing Na^+ and K^+, as well as the additional monovalent cation (X^+); and (c) solutions containing Na^+, K^+ and the divalent cation, X^{2+}. Defining $\alpha = \exp(-FV_r/RT)$ where V_r is the reversal potential, these equations are as follows.

$$\frac{P_K}{P_{Na}} = \frac{[Na^+]_i - \alpha[Na^+]_o}{\alpha[K^+]_o - [K^+]_i}, \quad (2)$$

$$\frac{P_X}{P_{Na}} = \frac{[Na^+]_i - \alpha[Na^+]_o}{\alpha[X]_o - [X]_i} + \frac{P_K}{P_{Na}}\left(\frac{[K^+]_i - \alpha[K^+]_o}{\alpha[X]_o - [X]_i}\right), \quad (3)$$

$$\frac{P_X}{P_{Na}} = \frac{1+\alpha}{4}\left(\frac{[Na^+]_i - \alpha[Na^+]_o}{\alpha^2[X]_o - [X]_i}\right) + \left(\frac{1+\alpha}{4}\right)\left(\frac{P_K}{P_{Na}}\right)\left(\frac{[K^+]_i - \alpha[K^+]_o}{\alpha^2[X]_o - [X]_i}\right). \quad (4)$$

V_r denotes the measured reversal potential. P_K/P_{Na} was determined from experiments using solution D, which contained 135 mM KCl, as the extracellular solution, and solution B as the intracellular solution. The P_K/P_{Na} value of 1·32, corresponding to the average from five separate patches, was used in eqns (3) and (4).

In these calculations, ion activities were used instead of concentrations. The ion activities were obtained by multiplying the concentrations by the activity coefficient of the ion. The mean activity coefficient of the salt was estimated from the following formula (Robinson & Stokes, 1965; their eqn (9·13)):

$$\log f^{\pm} = -\frac{A|z_1 z_2|\sqrt{I}}{1+\sqrt{I}} + bI, \quad (5)$$

where $f^{\pm}$ is the mean activity coefficient for the salt, A is a constant (0·5119 at 22 °C), z_1 and z_2 are valencies of the ions, and b is an adjustable parameter, which was calculated from tabulated activity coefficient data at 0·1 M (Robinson & Stokes, 1965; Weast, Astle & Beyer, 1985). I is the ionic strength of the solution. The activity coefficient for Ca^{2+} ions ($f_{Ca^{2+}}$) was estimated from the mean activity coefficient for the salt $CaCl_2$ (f_{CaCl_2}) using the Guggenheim convention (i.e. $f_{Ca^{2+}} = (f_{CaCl_2})^2$) (Shatkay, 1968; Butler, 1968). The same procedure was used for Mg^{2+}, and anions present at low concentrations (Hepes or glutamate) were treated as the Cl^- ions.

Given the ionizing constant (pK_a) of 9·337 for ammonium at 22 °C (Robinson & Stokes, 1965), 99·4 % of the total ammonium is expected to be ionized at pH 7·1. Therefore, no correction was made for the negligible amount of its non-ionized form.

In the plots of current–voltage relationships (Figs 1*B*, 2, 4, 5, 6 and 8), error bars were omitted to make these figures clearer. This is justified because most standard errors of the mean were smaller than the symbols used to plot the data points. In the other figures (Figs 3 and 9), tables and the text, data were all expressed as the means ± standard deviation and each error bar indicates size of the standard deviation.

Data fitting and evaluation of the model parameters

The current–voltage data were fitted to the equations of the model using a SIMPLEX minimization algorithm (Press, Flannery, Teukolsky & Vetterling, 1988). Since the program also gives an estimate of the errors, we have shown within parentheses the rate constants that were affected by a relative error of 30 % or greater (see the legends of Figs 2, 4, 5, and 6). Since the parameters in Table 3 were calculated using those rate constants, it is likely that all the quantities in Table 3 are affected by a relative error of at least 30 %.

RESULTS

General description of channel events

Figure 1*A* shows glutamate receptor single-channel currents recorded from an inside-out patch in symmetrical Na^+ (140 mM) and in the absence of divalent cations. The channel was activated by 10 mM monosodium L-glutamate in the pipette. Even with this high agonist concentration, the frequency of channel opening in the excised patch configuration was generally low. Approximately one out of seven patches showed channel openings that were sufficiently frequent to allow recordings to be taken in a wide range of membrane potentials. After excision in the inside-out configuration, the frequency of channel opening declined gradually, with virtual cessation of activity after

20 min. As illustrated in Fig. 1*A*, brief channel closures were more frequent for positive than negative membrane potentials (compare records at +80 and −80 mV, or at +40 and −40 mV), suggesting that the properties of the gating kinetics at depolarized membrane potentials are different from those in conditions of greater physiological relevance, such as near to the resting membrane potential. However, this point was not investigated further, since it was difficult to obtain enough channel openings with this patch configuration.

We also observed occasional opening events with lower conductances (50–70 % of the main state conductance). However, due to their low frequency, we did not study them systematically.

Current–voltage relations in NaCl solutions

Figure 1*B* shows the *I–V* relation obtained from the same patch as in Fig. 1*A*. The curve is almost linear between −80 and +100 mV, the single-channel conductance being 170·4 pS. In four other patches, the channels had similar characteristics with an average single-channel conductance of 157·6 ± 15·2 pS ($n = 5$). Assuming that the single-channel current is carried only by Na^+ (see below), the permeability, P_{Na}, as estimated by the GHK current equation (eqn (1)) is $3{\cdot}89 \pm 0{\cdot}38 \times 10^{-13}$ cm^3 s^{-1}.

The *I–V* relations observed in Fig. 2 refer to experiments in which Na^+ was decreased internally, while maintained constant externally (pipette). The data could not be fitted using the GHK current equation, especially at low $[Na^+]_i$. For example, at 17·5 mM NaCl and 120 mV membrane potential, the predicted current is 3·7 pA, in obvious disagreement with the experimental value of 9·7 ± 0·4 pA ($n = 4$).

The reversal potential was dependent on Na^+ but not on Cl^-

The first step in the characterization of the channel selectivity was to measure the reversal potential at various intracellular concentrations of NaCl (140, 70, 35 and 17·5 mM). To maintain osmolarity, decreases of the NaCl concentrations in the internal solution were compensated by additions of sucrose. In all cases, the external medium was the standard solution (solution A). The *I–V* relationships for the conditions specified above are plotted

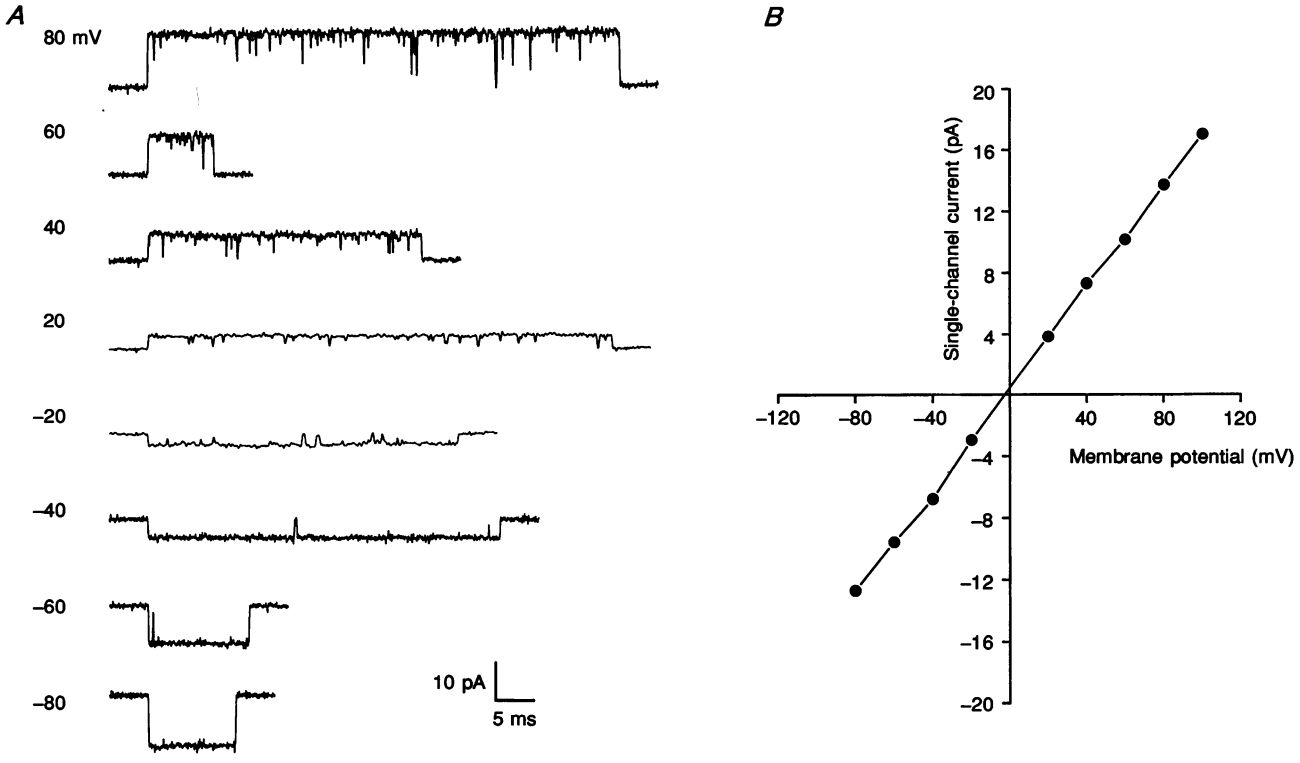

Figure 1. Single-channel currents induced by L-glutamate
A, sample tracings from a representative patch. All recordings were carried out in the inside-out patch configuration. The external solution was the standard extracellular solution (solution A). The internal solution was the standard intracellular solution (solution B). The extracellular solution contained 10 mM monosodium L-glutamate. Membrane potentials (in mV) are shown on the left side of the traces. Signals were low-pass filtered at 1 kHz for 20 and −20 mV membrane potentials and at 5 kHz for others. *B*, the *I–V* relation obtained from the same patch. Data points were connected by straight lines. Single-channel conductance was 170·4 pS in this patch. The standard error of each data point was smaller than the symbol.

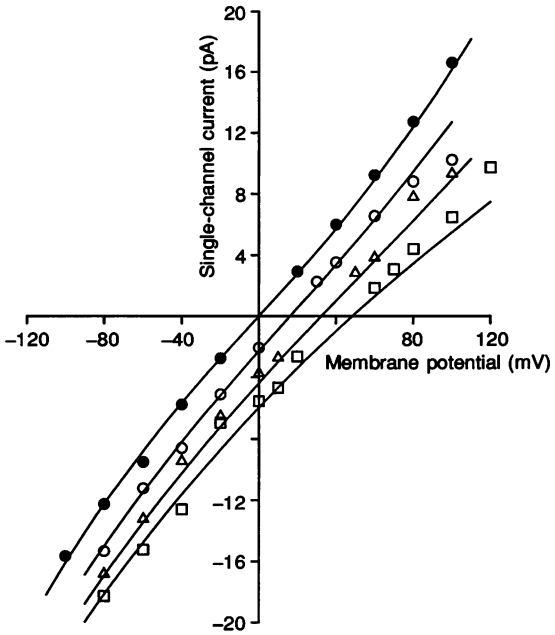

Figure 2. Single-channel current–voltage relations for various internal NaCl concentrations
The external solution was the standard extracellular solution (solution A). NaCl in the internal solution was replaced isosmotically with sucrose by mixing solutions B and C at an appropriate ratio. Results from different experiments were pooled for 140 mM NaCl ($n = 5$, ●), 70 mM NaCl ($n = 5$, ○), 35 mM NaCl ($n = 5$, △), and 17·5 mM NaCl ($n = 5$, □). Continuous lines are theoretical curves from the three-barrier model. The rate constants for Na^+, divided by 10^9 and listed in the order, $\bar{\rho}'$ (s^{-1} M^{-1}), $\bar{\lambda}'$ (s^{-1}), $\bar{\mu}'$ (s^{-1}), $\bar{\rho}''$ (s^{-1} M^{-1}), $\bar{\lambda}''$ (s^{-1}), $\bar{\mu}''$ (s^{-1}) are: 3·90, (0·18), 1·25, 1·18, (4·63) and 0·16. The numbers within parentheses are affected by errors greater than 30 % (as evaluated by the computer program). The 'electrical' distances between the energy wells (see Fig. 10), are: $\alpha = 0{\cdot}24$, $\beta = 0{\cdot}20$, $\gamma = 0{\cdot}56$.

in Fig. 2, which shows that dilution of intracellular NaCl causes displacement of the reversal potential in the positive direction, implying that the channel is more permeable to Na^+ than to Cl^-.

Figure 3 shows the reversal potential at different Na^+ activities in a semilogarithmic plot (○). The slope, 46·7 mV for a 10-fold reduction of the Na^+ activity, is lower than would be expected if Na^+ were the sole permeant ion (58·5 mV per decade at 22 °C), thus suggesting that other ions may contribute to the reversal potential, notably K^+ and Cl^-. (A low concentration of K^+ was kept in the internal solution, since it seemed to prolong the life of the preparation.) As is described below, K^+ was slightly more permeant than Na^+, with a P_K/P_{Na} of about 1·32, suggesting that for a more accurate estimate of the cation selectivity of the channel, the term $(P_K/P_{Na}) \times [K^+]_i$ must be added to $[Na^+]_i$ in the Nernst equation. By doing so, the slope of the plot increased to 56·5 mV for a 10-fold variation of ion activity (● in Fig. 3), which is almost the theoretical value for ideal selectivity to cations, thus demonstrating that the channel permeability to Cl^- must be very low.

Since the value of the reversal potential is more sensitive to P_{Cl}/P_{Na} when the ionic gradient is high, we have obtained an estimate for the upper limit of P_{Cl}/P_{Na} from the reversal potential at 17·5 mM $[NaCl]_i$. The mean value of this potential was 39·53 mV, with a standard error of 0·92 mV. From Student's t distribution, the reversal potential is estimated to be in the range of 37·58–41·49 mV, with 95 % confidence. On the other hand, using P_{Cl}/P_{Na} values of 0·03 and 0·04, the reversal potentials predicted from the constant field theory were 38·41 and 37·35 mV, respectively, thus indicating that P_{Cl}/P_{Na} is smaller than 0·04.

Current–voltage relations with various monovalent cations

In order to study the permeabilities for monovalent cations other than Na^+, NaCl and KCl in the standard external solution were replaced with LiCl, KCl, RbCl, CsCl or NH_4Cl, while internally solution B was used in all cases. The relative

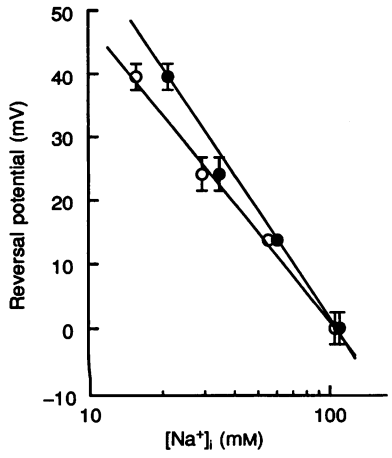

Figure 3. Dependence of reversal potentials on $[Na^+]_i$
The reversal potential was estimated by linear interpolation, using the same data as in Fig. 2. Each symbol represents results from 5 separate patches. Vertical bars indicate standard deviations (shown only when they are larger than the symbol used). Reversal potentials were plotted against the corrected (●) or uncorrected (○) intracellular Na^+ activity. Correction for Na^+ activity, taking K^+ into account, was made by adding $(P_K/P_{Na}) \times [K^+]_i$ to $[Na^+]_i$. The value of 1·32 was used for P_K/P_{Na}. Data were fitted by straight lines, with slopes of 46·7 (○) and 56·5 mV per decade (●). Room temperature, 21–23 °C.

Table 2. Summary of experiments with various extracellular monovalent cations

Cation	Reversal potential (mV)	P_X/P_{Na}	Measured I_{-60} (pA)*	Predicted I_{-60} (pA)
Li^+	−12·58 ± 1·20	0·57 ± 0·03	−5·63 ± 0·30	−5·39
K^+	5·79 ± 1·95	1·32 ± 0·10	−15·54 ± 0·45	−12·05
Na^+	0·02 ± 2·40	1·00	−9·48 ± 0·33	−9·46
Rb^+	2·32 ± 0·74	1·15 ± 0·04	−15·26 ± 0·64	−10·61
Cs^+	0·78 ± 0·52	1·09 ± 0·03	−14·25 ± 0·59	−9·89
NH_4^+	3·38 ± 1·01	1·18 ± 0·05	−18·23 ± 0·98	−11·01
Mg^{2+}	1·37 ± 2·76	2·31 ± 0·62	−3·39	−16·34
Ca^{2+}	17·55 ± 2·79	9·55 ± 2·05	−4·04	−51·94

*I_{-60} means a single-channel current at membrane potential of −60 mV. All values are means ± standard deviation. External solution contained either one monovalent cation (135 mM; solution D) or an isotonic mixture of Na^+ and a divalent cation (45 mM; solutions A, E and F). All data for monovalent cations are from 5 different experiments, while I_{-60} for each divalent cation was from a single patch. Predicted I_{-60} was calculated from P_X/P_{Na}, using the Goldman–Hodgkin–Katz current equation.

permeabilities of these cations with respect to Na^+, as estimated from the reversal potential, are listed in Table 2. Although the following sequence could be determined: $K^+ > NH_4^+ \approx Rb^+ > Cs^+ > Na^+ > Li^+$, the differences in the permeability ratios were small, except for Li^+.

The *I–V* curves, with the test cations in the external medium and Na^+ in the internal one, are plotted in Fig. 4. As can be seen, there were pronounced differences in the inward currents, despite the similarity of the reversal potentials. From the currents measured at −60 mV, which are listed in Table 2, one can see that the decreasing order of their amplitudes, $NH_4^+ > K^+ \approx Rb^+ > Cs^+ > Na^+ > Li^+$, is similar, but not identical, to that of the permeability ratios, a result that is at variance with the GHK theory. Even more obvious discrepancies can be seen by comparing the measured values for various inward currents at −60 mV with those predicted by the GHK equation (see the last column of Table 1). Although there was a reasonable agreement in the case of Na^+ and Li^+, for all the other cations the measured values were much larger than the theoretical ones.

The outward currents in Fig. 4 were found to be virtually independent of the test cation, as expected from the fact that the intracellular solution was the same in all experiments.

Current–voltage relations with various Mg^{2+} and Ca^{2+} concentrations

The effects of Mg^{2+} and Ca^{2+} on the channel electrical properties were studied by varying the extracellular concentrations of these ions between 2·25 and 45 mM. Addition of Mg^{2+} and Ca^{2+} salts was compensated for by reduction of NaCl to maintain osmolarity. The standard internal solution (solution B) was used in all experiments. At high extracellular concentrations of either Mg^{2+} or Ca^{2+} (45 mM), the frequency of channel opening became very low, possibly because of chelation of glutamate by these divalent cations or some effects of these ions on the gating kinetics of the channel.

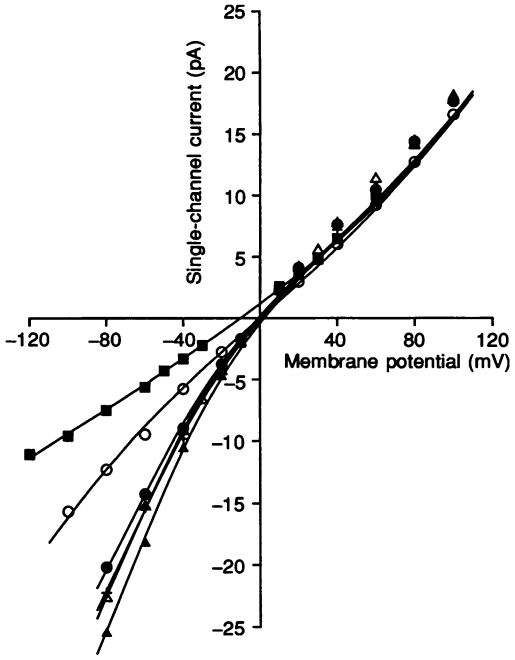

Figure 4. Single-channel current–voltage relations with various extracellular monovalent cations
The external solution contained 135 mM XCl, 10 mM monosodium L-glutamate, and 5 mM Hepes (sodium salt, pH 7·1), where X denotes Li^+, Na^+, Cs^+, Rb^+, K^+ or NH_4^+ (solution D). The internal solution was the standard intracellular solution (solution B). Results from five separate patches are pooled for Li^+ (■), Na^+ (○), Cs^+ (●), Rb^+(△), K^+ (+), and NH_4^+ (▲). Continuous lines are theoretical curves from the three-barrier model. The rate constants for the monovalent cations other than Na^+, divided by 10^9, and given in the same units and order as those in the legend of Fig. 2, are: [Li^+], 0·56, 0·27, 0·86, 7·10, 0·21, 0·085; [K^+], 0·87, 1·24, (32·1), (62·7), 3·45, 0·16; [Rb^+], 0·79, 1·42, (39·04), (66·28), 3·95, 0·17; [Cs^+], 0·82, 1·06, (30·0), (57·7), 3·01, 0·15; [NH_4^+], (1·04), (0·91), (53·0), (49·9), (5·58), (0·18). See legend of Fig. 2 for meaning of parentheses around some numbers. α, β and γ are same as in Fig. 2.

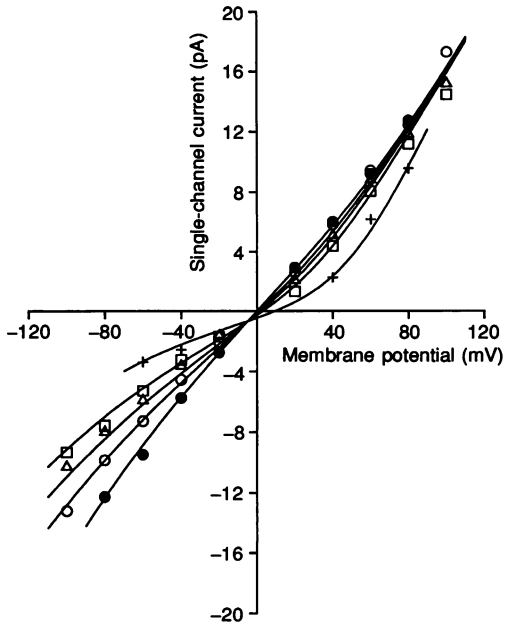

Figure 5. Single-channel current–voltage relations in the presence of different external Mg^{2+} concentrations
$[Mg^{2+}]_o$ ranged from 0 to 45 mM. Internal solution is the standard solution (solution B). Results from different patches are pooled for 45 mM Mg^{2+} ($n = 2$, +), 9 mM Mg^{2+} ($n = 5$, □), 4·5 mM Mg^{2+} ($n = 5$, △), 2·25 mM Mg^{2+} ($n = 5$, ○), and 0 mM Mg^{2+} ($n = 5$, ●). Continuous lines are theoretical curves from the three-barrier model. The rate constants for Mg^{2+}, divided by 10^9, and given in the same units and order as those in the legend of Fig. 2 are: 12·23, (0·18), 0·0015, 4·84, (0·029), 0·023. See legend of Fig. 2 for meaning of parentheses around numbers. α, β and γ are same as in Fig. 2.

At 45 mM of Mg^{2+} and Ca^{2+}, the reversal potentials were 2·6 and 19·2 mV, respectively. This indicates that both ions are permeant through the channel, since the reversal potential would be expected to be at −16·5 mV, if Na^+ were the sole permeant ion. The relative permeabilities of Mg^{2+} and Ca^{2+} with respect to Na^+, as calculated from the reversal potential for mixtures of divalent and monovalent cations, were $2{\cdot}31 \pm 0{\cdot}62$ ($n = 2$) and $9{\cdot}55 \pm 2{\cdot}05$ ($n = 2$), respectively (Table 2).

The *I–V* relations in Figs 5 and 6 indicate that the presence of either of these divalent ions in the external solution lowers the amplitude of both inward and outward currents. The reduction of the outward current was small but unambiguous, especially at high divalent cation concentrations (+ in Figs 5 and 6). Again, this effect cannot be reconciled with the classic constant field theory, since the limiting outward current, according to that theory, should be completely determined by Na^+, the sole permeant cation in the internal solution. Instead, at high external concentrations of divalent cations, a substantial reduction of the outward current was observed even at voltages as high as +80 mV.

The reduction of the inward current with Mg^{2+} and Ca^{2+} present was even more pronounced than that of the outward current, the effect being clear even at low concentrations (2·25 mM, ○ in Figs 5 and 6). This finding is again incompatible with the constant field theory. In fact, considering that P_{Ca}/P_{Na} and P_{Mg}/P_{Na} were greater than one, the currents in the presence of these divalent ions would be expected to be larger than in their absence.

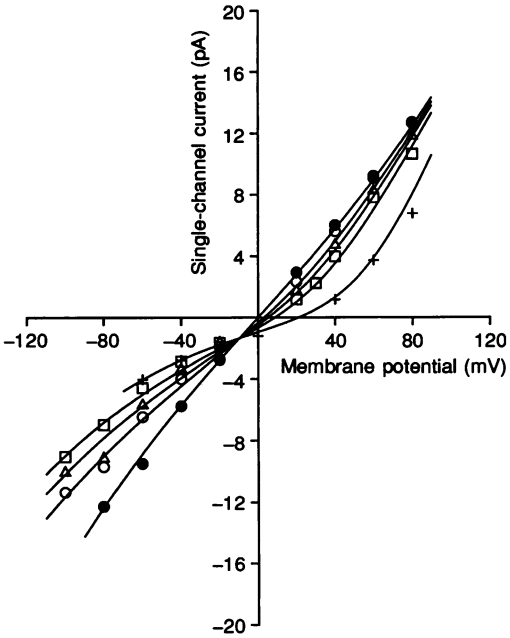

Figure 6. Single-channel current–voltage relations in the presence of different external Ca^{2+} concentrations
$[Ca^{2+}]_o$ ranged from 0 to 45 mM. Internal solution is the standard solution (solution B). Results from different patches are pooled for 45 mM Ca^{2+} ($n = 2$, +), 9 mM Ca^{2+} ($n = 5$, □), 4·5 mM Ca^{2+} ($n = 5$, △), 2·25 mM Ca^{2+} ($n = 5$, ○), and 0 mM Ca^{2+} ($n = 5$, ●). Continuous lines are theoretical curves from the three-barrier model. The rate constants for Ca^{2+}, divided by 10^9, and given in the same units and order as those in the legend of Fig. 2 are: (33·61), (0·18), (0·002), (12·50), (0·024), (0·04). See legend of Fig. 2 for meaning of parentheses around numbers. α, β and γ are same as in Fig. 2.

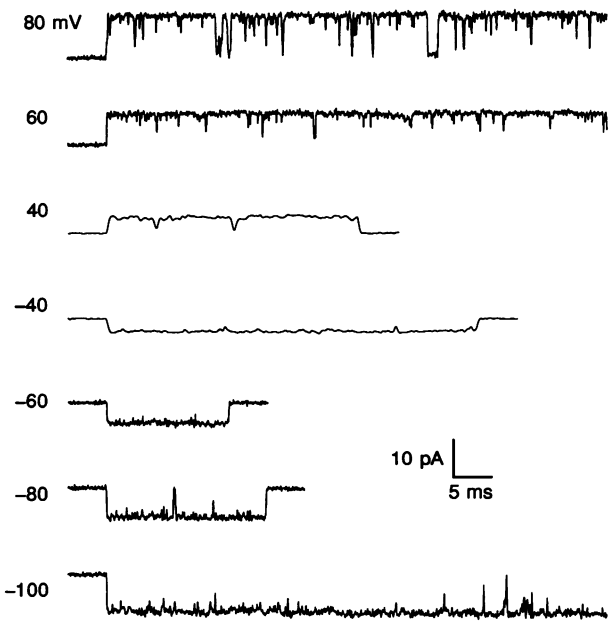

Figure 7. Sample tracings of single-channel currents in the presence of external Mg^{2+}
The external Mg^{2+} concentration was 9 mM. The internal solution was the standard solution (solution B). The membrane potential (in mV) is shown at the left of each trace. Traces were low-pass filtered at 1 kHz (+20 and −20 mV membrane potential) or 5 kHz (all other traces).

Instead, at 45 mM and −60 mV, while the predicted currents were −16·34 pA for Mg^{2+} and −51·94 pA for Ca^{2+}, the measured ones were only −3·39 pA and −4·04 pA, respectively (Table 2). These data clearly suggest that the divalent cations tested interfere with the Na^+ current by strongly interacting with some molecular component of the channel.

It is known that Mg^{2+} blocks the NMDA(*N*-methyl-D-aspartic acid)-type glutamate receptor channels (Nowak *et al.* 1984; Mayer *et al.* 1984). However, the reduction of the inward current by extracellular Mg^{2+} in the *Drosophila* glutamate receptor channel cannot be attributed to simple block, since the reversal potential indicates that the ion is actually quite permeant. Differences between the effects of Mg^{2+} on the NMDA receptor channel and the present channel are seen also in the behaviour of the open channel noise. As is shown in Fig. 7, the noise of both the outward and inward currents in the presence of extracellular Mg^{2+} (9 mM) is similar to that in the absence of Mg^{2+} (see Fig. 1*A*). This behaviour of the noise differs from that observed in NMDA channels, where extracellular Mg^{2+} induces conspicuous flickering noise in the inward current (Nowak *et al.* 1984; Ascher & Nowak, 1988).

The unitary conductance saturates at high concentrations of Na^+

Using symmetrical solutions with Na^+ as the sole permeant ion, the 'zero current' channel conductance was studied as

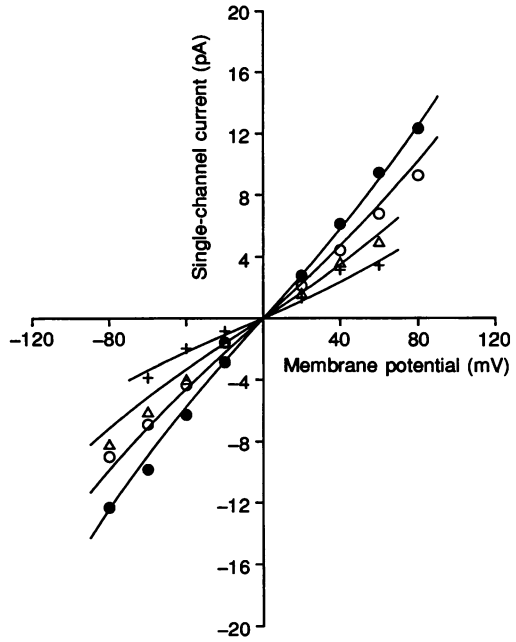

Figure 8. Single-channel current–voltage relations with various symmetrical Na^+ concentrations
Equal intracellular and extracellular Na^+ concentrations. Concentration of Na^+ was reduced by replacement with sucrose. Results from different patches were pooled for 145 mM [Na^+] ($n = 5$, ●), 72·5 mM Na^+ ($n = 3$, ○), 36·25 mM Na^+ ($n = 4$, △), and 18·25 mM Na^+ ($n = 2$, +). Continuous lines are theoretical curves from the three-barrier model.

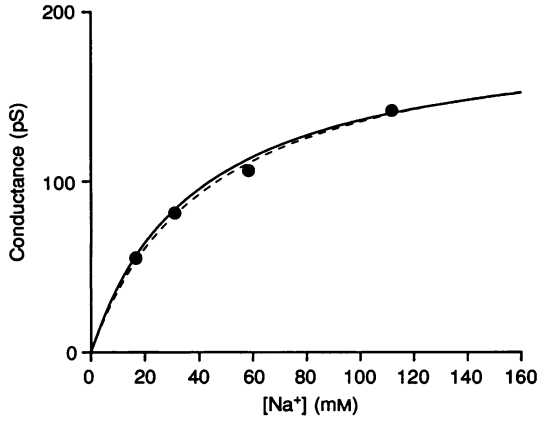

Figure 9. Conductance–activity relation for Na^+
The slope conductances were determined from the data in Fig. 8 by linear interpolation between the mean single-channel currents near 0 mV membrane potential, and were plotted against Na^+ activity. The continuous line represents the best fit obtained (independently of the model) from the hyperbolic relation,

$$g_0 = g_{max}\left(\frac{[Na^+]}{[Na^+] + K_M}\right)$$

where g_0 denotes single-channel conductance, g_{max} is 195·4 pS and K_M is 44·6 mM. The dashed line shows the theoretical prediction from our model, eqns (13), (14) and (15), using the values of the constants for Na^+ shown in Table 3.

a function of ion activity. Decreases of the NaCl concentration on both sides were compensated for by additions of sucrose to maintain osmolarity. The *I–V* relationships, shown in Fig. 8, were determined for each of the NaCl concentrations tested. The curves were found to be approximately linear over a fairly wide range of voltages, and the reversal potential was close to zero, as expected. Due to the linearity of the curves, the values of the conductance were almost independent of the voltage at which they were estimated. The plot of the conductance as a function of Na^+ activity is illustrated in Fig. 9, where one can see that the data points do not lie on a straight line, but are well fitted by a Michaelis–Menten equation, similar to eqn (13), where g_0, in that equation, is the single-channel conductance, g_{max} its asymptotic value at high ion activities, and K_M the half-saturating activity of the permeant ion. The best fit, shown by a continuous line in Fig. 9, was obtained for $g_{max} = 195{\cdot}4$ pS and $K_M = 44{\cdot}6$ mM. As it will be emphasized later (Discussion), almost equal values are obtained from the rate constants deduced by fitting the independently obtained *I–V* relations (Fig. 2) with an Eyring model.

A one-ion, three-barrier pore as a model for the glutamate receptor channel

The simplest model for the channel that gave a good fit to the data was a 'one-ion, three-barrier' model based on the Eyring rate theory (Läuger, 1973). In the presence of two permeant ions, for example, Na^+ and X (where X can be any of the other test cations), five states of occupancy are possible, as is shown in Fig. 10*B*. Once the probabilities of these states are evaluated (see Appendix), the steady-state fluxes of Na^+ (j_{Na}) and X (j_X) can be expressed by:

$$j_{Na} = \lambda'_{Na}\, p_2 - \lambda''_{Na}\, p_3, \quad (6)$$

$$j_X = \lambda'_X\, p_4 - \lambda''_X\, p_5, \quad (7)$$

where p_i denotes the probability of state i, λ' and λ'' denote the rate constants for crossing the central barrier, and the indices $'$ and $''$ (when applied to rate constants) denote outward and inward direction, respectively. The meaning of the remaining rate constants, υ', υ'', μ', and μ'' should be apparent from the diagram in Fig. 10*A*.

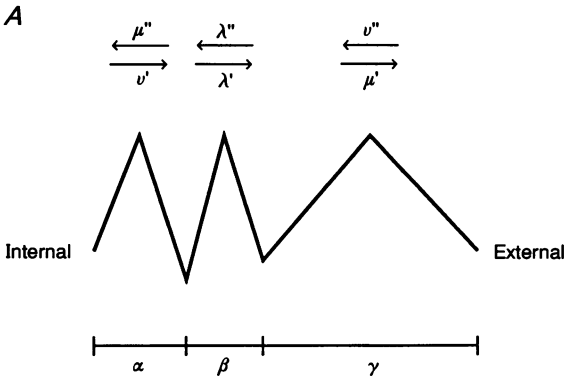

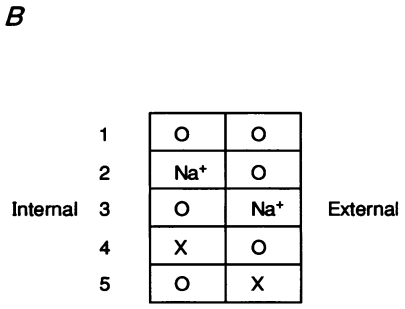

Figure 10. Diagrams of the three-barrier, two-site model
A, a three-barrier, two-site model for the channel. Approximate energy profile for Na^+. The rate constants depend on the applied voltage, and two of them, υ' and υ'', on ion activity (see eqns (8) and (9)). *B*, states of ion occupancy for a 'one-ion' channel in the presence of two permeant ions, Na^+ and X.

Table 3. Parameters of the model

	K_M (mM)	g_{max} (pS)	P_X/P_{Na}
Li^+	68	172	0·54
Na^+	40	189	1·00
K^+	135	654	1·01
Rb^+	157	698	0·93
Cs^+	135	609	0·94
NH_4^+	149	806	1·14
Mg^{2+}	0·27	22·6	4·46
Ca^{2+}	0·14	30·8	11·4

Theoretical values of K_M, g_{max} and P_X/P_{Na} calculated using eqns (12), (14) and (15) and the rate constants in the legends of Figs 2, 4, 5 and 6. See the last section of the Methods for comments on the parameters' errors.

For simplicity, and in order to reduce the number of adjustable parameters, the following assumptions have been used: (1) the profile of the electric potential is linear between adjacent sites; (2) the peaks of the barriers are half-way between adjacent energy wells; and (3) only one ion can be present in the channel at the time.

The dependence of the rate constants on voltage is then

$$\upsilon' = \bar{\upsilon}' \exp\left(z\alpha\frac{\phi}{2}\right), \quad \lambda' = \bar{\lambda}' \exp\left(z\beta\frac{\phi}{2}\right), \quad \mu' = \bar{\mu}' \exp\left(z\gamma\frac{\phi}{2}\right),$$
$$\upsilon'' = \bar{\upsilon}'' \exp\left(-z\alpha\frac{\phi}{2}\right), \quad \lambda'' = \bar{\lambda}'' \exp\left(-z\beta\frac{\phi}{2}\right), \quad \mu'' = \bar{\mu}'' \exp\left(-z\gamma\frac{\phi}{2}\right), \quad (8)$$

where ϕ denotes the total membrane potential in units of RT/F, α, β and γ $(=1-\alpha-\beta)$ are the fractional 'electrical' distances between the energy wells (the mouths of the channels also being considered as energy wells), z is the valency, and the bars over the symbols designate the voltage-independent factors in the rate constants. Also, recalling that the rate constants for entering the channel are proportional to the ion activities, we have:

$$\bar{\upsilon}' = \bar{\rho}'\, a_i, \qquad \bar{\upsilon}'' = \bar{\rho}''\, a_o, \quad (9)$$

where a_i and a_o denote the intracellular and the extracellular ion activities, respectively. (See Läuger, 1973 for a physical interpretation of the rate constants, ρ' and ρ''.)

Taking into account the condition of 'microscopic reversibility', namely

$$\bar{\rho}'\bar{\lambda}'\bar{\mu}' = \bar{\rho}''\bar{\lambda}''\bar{\mu}'', \quad (10)$$

it is apparent that only five of the six rate constants in eqn (10) are independent. Using the method described in the Appendix to evaluate the probabilities of the states of occupancy of the channel, and substituting their values in eqns (6) and (7), one finds explicit expressions for the fluxes and the single-channel current. Since the equations are somewhat lengthy, they are given in the Appendix, eqns (A4) and (A7). Equation (A4) refers to the case of only one permeant ion, Na^+, and eqn (A7) to the particular case of a mixture of two ions (the only one relevant to our experiments), in which one of the two ions is present only in the external solution. All the continuous curves in Figs 2,4,5,6 and 8 are derived from eqns (A4) and (A7), and the fitting values of the rate constants are given in the appropriate figure legends.

Equation (A4) has been used to deduce all the constants for Na^+, as well as the two parameters that define the location of the two internal energy wells, α and β. These values have then been substituted in eqn (A7) in order to fit the data for mixtures of Na^+ with other ions.

Permeability ratios and Eyring theory

In models for ion transport based on Eyring theory, the concept of permeability ratio is slightly less simple than in the GHK theory. From eqns (A4) and (A7) in the Appendix, one can see that the closest counterpart to the standard GHK permeability ratio, P_X/P_{Na}, is the quantity:

$$\frac{P_X}{P_{Na}} = \frac{P_X(1)}{P_{Na}(1)}\left(\frac{Q_{Na}}{Q_X}\right), \quad (11)$$

where $P_{Na}(1)$ and Q_{Na} are defined in eqns (A5) and (A6), and $P_X(1)$ and Q_X are the corresponding quantities for ion X. Since Q_{Na} and Q_X are voltage dependent, so generally will be the permeability ratio in eqn (11). However, eqn (11) acquires a simple meaning when the reversal potential is very small, as it would be, for example, in the 'quasi-equilibrium' condition, in which the concentration of one of the two ion species, e.g. Na^+, would be the same on both sides of the membrane and ion X would be present in only one solution at very low concentration. In this case, the reversal potential would be small and, as one can see by analysing eqns (A4), (11) and (13), the permeability ratio, as defined in eqn (11), would be related to the ratio of the channel conductances in symmetrical single-salt solutions by:

$$\frac{P_X}{P_{Na}} = \left(\frac{z_{Na}^2}{z_X^2}\right) \lim_{(a_X = a_{Na}) \to 0} \left(\frac{g_o(X)}{g_o(Na)}\right)$$
$$= \left(\frac{z_{Na}^2}{z_X^2}\right)\left(\frac{g_{max}(X)}{g_{max}(Na)}\right)\left(\frac{K_M(Na)}{K_M(X)}\right), \quad (12)$$

where g_{max} and K_M are defined in eqns (15) and (14), respectively.

A comparison between the permeability ratios calculated from eqn (12) (using g_{max} and K_M values of Table 3), and those determined directly from reversal potential, can be made by inspecting Tables 2 and 3. The two sets of numbers are quite close, even though the direct measurements of P_X/P_{Na}, shown in Table 2, were not always performed in 'quasi-equilibrium' conditions. The good agreement is not surprising, however, since the dependence of the permability ratios on voltage is generally not very steep.

DISCUSSION

The purpose of this study was to describe the single-channel ion permeation properties of the glutamate receptor channel in cultured myotubes of *Drosophila* embryos. The experiments demonstrated that the channel is permeable to several monovalent cations, as well as to Ca^{2+} and Mg^{2+}, the only divalent cations tested in this study. Although the data are straightforward, certain features of the results and of the model deserve further discussion. We calculated the permeabilities for the various cations using the GHK equation, because many previous workers describe their results in terms of that model. In the following section, we compare our results with those of previous reports concerning several types of glutamate receptor channels as well as ACh receptor channels. However, since the constant field theory failed to account for most of the experimental results, in the remaining part of the Discussion we provide some comments about certain properties of our three-barrier model and its appropriateness for describing the data in this paper.

Comparison with previous reports

Jan & Jan (1976*a*, *b*) studied the ion permeabilities of the glutamate receptor channel at the neuromuscular junction of *Drosophila* larvae, using the conventional microelectrode technique. They found that the channel was cation selective, permeable to Na^+, K^+ and Mg^{2+}, but not to Cl^-. Our results confirm and extend their findings at the single-channel level. The only major discrepancy is the effect of Ca^{2+}, which they reported to be impermeant, while our results strongly point to the contrary. The reason for this difference is unknown.

The weak selectivity among alkali cations observed in the glutamate receptor channel in *Drosophila* seems to be a general characteristic of ligand-gated cation-selective ion channels, such as various types of ACh receptor channels (Lassignal & Martin, 1977; Huang, Catterall & Ehrenstein, 1978; Linder & Quastel, 1978; Adams, Dwyer & Hille, 1980), as well as glutamate receptor channels (Anwyl, 1977*a*; Dekin, 1983). However, permeabilities to divalent cations differ considerably among those channels. Mg^{2+} permeates through the nicotinic ACh receptor channel (Adams *et al.* 1980; Dani & Eisenman, 1987), but blocks the NMDA-type glutamate receptor channel (Nowak *et al.* 1984; Mayer *et al.* 1984). Ca^{2+} permeates through ACh receptor channels (Lassignal & Martin, 1977; Bregestovski, Miledi & Parker, 1979; Adams *et al.* 1980; Decker & Dani, 1990), the NMDA-type glutamate receptor channel (Mayer & Westbrook, 1987*b*; Ascher & Nowak, 1988; Iino, Ozawa & Tsuzuki, 1990), the glutamate receptor channel at the arthropod neuromuscular junction (Anwyl, 1977*b*; Dekin, 1983). As for non-NMDA types of glutamate receptor channel, some are reported to be permeable to Ca^{2+} (Iino, Ozawa & Tsuzuki, 1990; Gilbertson, Scobey & Wilson, 1991), but other types are not (Mayer & Westbrook, 1987*b*; Iino *et al.* 1990). If the role of these channels is solely to depolarize the membrane potential, their diverse permeabilities to divalent cations would have no obvious significance. However, there are reasons to believe that the unique characteristics of the permeability to divalent cations of certain channels might be physiologically meaningful. For example, block by Mg^{2+} endows the NMDA channel with voltage-dependent responsiveness (Nowak *et al.* 1984; Mayer *et al.* 1984), and calcium influx through the NMDA receptor has been implicated in excitotoxicity (Rothman & Olney, 1987). Our results show that both Ca^{2+} and Mg^{2+} permeate through the glutamate receptor channel in embryonic *Drosophila* muscle with high permeabilities relative to Na^+ ($P_{Ca}/P_{Na} = 9{\cdot}55$; $P_{Mg}/P_{Na} = 2{\cdot}31$). The physiological role of this permeability to divalent cations is of interest and deserves further investigation.

Reduction of the conductance of monovalent cations by permeant divalent cations has been reported for various types of ACh receptor channels (Marchais & Marty, 1979; Magleby & Weinstock, 1980; Dani & Eisenman, 1987; Decker & Dani, 1990; Neuhaus & Cachelin, 1990; Ifune & Steinbach, 1991), as well as for the NMDA-type glutamate receptor channel (Mayer & Westbrook, 1987*b*; Ascher & Nowak, 1988). Most investigators attempted to explain the phenomenon using a two-barrier, one-site rate-theory model and/or postulating the presence of negative surface charges.

Why an Eyring model?

Most of the data presented in this paper were inconsistent with the classic model based on integration of the Nernst–Planck equation and the assumption of 'constant field' (GHK theory). First, decreasing the intracellular NaCl activity resulted in changes of the reversal potential according to the Nernst equation for cations, but the current amplitudes were larger than predicted from the GHK equation. Second, in mixtures of Na^+ with other monovalent cations, the currents were again much larger than expected from the permeability ratios estimated by reversal potential. Third, in mixtures of Na^+ with Ca^{2+} and Mg^{2+}, the reversal potential indicated a higher permeability to the divalent cations than to Na^+, but the current amplitudes, inward as well as outward, were clearly lower in the presence of these ions. Fourth, in

symmetrical Na^+ solutions, the dependence of the 'zero-current' conductance on Na^+ activity was not linear.

Given the inadequacy of the GHK theory to account for the data, we have used an alternative model based on the Eyring rate theory and the assumption of one-ion occupancy of the channel.

Recently, the use of the Eyring theory for describing ion fluxes has been criticized on the grounds that some of its basic assumptions are unlikely to hold in membrane channels (Cooper, Gates & Eisenberg, 1988). This criticism is probably legitimate, and one should therefore be cautious about interpreting too literally the information derived from that theory. However, despite its shortcomings, and as long as the molecular strucure of the channels is unknown, the Eyring theory remains a very valuable tool for deducing first-approximation guesses about important transport properties of membrane channels.

As is well known, in the Eyring theory a channel is schematized as a sequence of free-energy barriers and wells (sites). Quasi-linear I–V relationships, such as we observe in this channel when Na^+ is the sole permeant ion, require at least three barriers, since only one or two would predict supra-linear I–V curves, steeper than indicated by the data.

Unfortunately, but inevitably, a three-barrier model for a channel has several parameters: five independent rate constants for each ion, and a minimum of two additional parameters to locate the energy peaks and wells in the electric field, if one assumes (as we do) that the peaks are half-way between adjacent sites.

The channel conductance in pure Na^+ solutions

Using eqn (A4), derived from Eyring's theory, to fit the I–V curves for different activities of internal Na^+ (see Fig. 2), we deduced the constants listed in the legend of Fig. 2. Since these parameters define all the steady-state electrical properties in pure Na^+ solutions, one test of the consistency of the model was to check whether these parameters fitted the 'zero-current' conductance as a function of Na^+ activity in symmetrical solutions, which was determined by an independent set of experiments. From eqn (A4), the 'zero-current' conductance for symmetrical Na^+ solutions is found to be:

$$g_0 = \lim_{V \to 0} \left(\frac{I}{V}\right) = g_{max}\left(\frac{a}{a + K_M}\right), \tag{13}$$

where

$$K_M = \frac{\bar{\mu}'\bar{\mu}''}{\bar{\rho}'\bar{\mu}' + \bar{\rho}''\bar{\mu}''}, \tag{14}$$

and

$$g_{max} = \frac{z^2 e^2}{kT}\left(\frac{\bar{\lambda}'\bar{\lambda}''}{(\bar{\lambda}' + \bar{\lambda}'')(\bar{\lambda}'/\bar{\mu}'' + \bar{\lambda}''/\bar{\mu}' + 1)}\right). \tag{15}$$

where k is Boltzmann's constant.

Using the values for the constants in the legend of Fig. 2, one finds: $g_{max} = 190$ pS and $K_M = 39{\cdot}6$ mM. Figure 9 shows good agreement between the data and the theoretical curve (dashed line) predicted using these values. A good agreement between theory and data is also shown in Fig. 8 for three of the four I–V relationships in symmetrical Na^+ solutions. Here again, the continuous curves are completely determined by the constants estimated by fitting the data in Fig. 2. The values of the two parameters that define the position of the sites, α and β, i.e. 0·24 and 0·20, respectively, indicate that the energy wells are not uniformly spaced, both being relatively close to the intracellular medium.

Although these parameters may, in principle, differ for each ion, we thought it reasonable to postulate that they represent an intrinsic feature of the channel, so that the same values for α and β were used for all the cations, monovalent as well as divalent.

Note in Table 3 that K_M for Na^+ is rather low as compared to that for the other monovalent cation. This suggests that the degree of channel occupancy by Na^+ will be substantial even at fairly low activities of this ion in solution, which explains why the slope of the outward current in Fig. 2 is not very sensitive to the level of intracellular Na^+. An alternative explanation might be a surface charge near the inner mouth of the channel. However, as we argue later in greater detail, in this case, one would also expect a tendency for the 'zero-current' conductance to approach non-zero values when the ion concentration is very low. Although experiments with very low Na^+ were difficult to perform, the data in Fig. 9 do not suggest such a trend.

Interaction of Na^+ with other monovalent cations

The effects of monovalent cations other than Na^+ were also studied, although in less detail. Figure 4 illustrates the I–V relationships for the case in which the test cation was in the outer solution (the pipette) and Na^+ inside, at similar concentrations. The data have been fitted with eqn (A7), where, of course, the constants referring to Na^+ and to the location of the sites were fixed at the values estimated previously from the data in Fig. 2. The permeabilities of most of the tested cations, as estimated from the reversal potential, were similar to that of Na^+, except for Li^+. By contrast, the amplitudes of the inward currents were considerably higher. This finding is incompatible with the GHK equation, as we have already mentioned, but is consistent with our model, since in models for ion permeation based on the Eyring theory, the permeability ratios and the conductance ratios are generally determined by different functions of the rate constants and of the voltage.

Effects of Ca^{2+} and Mg^{2+}

In Figs 5 and 6, the reversal potentials indicate that the permeabilities of Mg^{2+} and Ca^{2+} are higher than that of Na^+, although the levels of the current suggest that these ions also reduce the Na^+ current. The values of K_M for Ca^{2+} and Mg^{2+} are about two orders of magnitude lower than for Na^+ (see Table 3), which explains their ability to reduce the Na^+ current, and is not inconsistent with the reversal potential data, since the permeability ratios measured using such potentials are known to be independent of the ion-binding constants of the energy wells in the channel (Hille, 1975). Figures 5 and 6 show that both divalent cations also have the effect of displacing the outward Na^+ current toward more positive potentials. Similar results for the NMDA receptor in the presence of external Ca^{2+} have been reported by Ascher & Nowak (1988), and have been accounted for by postulating the presence of a surface charge on the external side of the membrane. Although we discuss the effects of surface charges in the next section, we would like to emphasize here that we do not need to invoke this assumption in order to explain the displacement of the Na^+ current by Ca^{2+} in our experiments with the *Drosophila* glutamate receptor channel. According to our model, increasing the external Ca^{2+} concentrations simply increases the probability of channel occupancy by this ion, and, since the Ca^{2+}-binding sites are in a region sensitive to the electric field, higher positive voltages are thus required to reduce that probability, unblock the channel and allow Na^+ to move in the outward direction at the same rate as in the absence of Ca^{2+}.

It is also relevant to point out that the data presented in Figs 5 and 6 can be viewed as the results of 'mole fraction' experiments, namely the type of experiments that are generally performed in order to test whether a channel is a one-ion or a multi-ion channel. Even though it was very difficult to measure the channel conductance at divalent ion concentrations higher than 50 mM, and thus to complete the 'mole fraction' experiment, the lack of minima for the conductance in the concentration range examined, and the fact that the I–V relationships for different ion mixtures are well described by our model, lend support to our assumption that the channel is a one-ion channel, at least for certain ion species.

Effects of surface charge

As we have mentioned already, some features of our data (e.g. the weak dependence of the I–V slope on internal Na^+, or the strong dependence of the reversal potential on external Ca^{2+}), although well explained by our model, may nevertheless suggest alternative interpretations in terms of surface charges.

Thus, assuming the validity of the Gouy–Chapman theory, we have developed an argument in order to estimate an upper limit for the surface charge density in our preparation. Our reasoning starts from a result of the Gouy–Chapman theory, according to which, in the presence of surface charges, the ion concentration at the membrane–solution interfaces remains finite even if its concentration in the bulk solution is reduced to vanishingly small levels (see, e.g. McLaughlin, 1989). In this case, if one assumes that the effects of the charges reach as far as the mouth of the channel, the conductance of the channel should stay above a non-zero limit at high dilution. We denote this limiting value by g_{lim}, whose theoretical expression, for a uniform and symmetrical surface charge density, is given by eqn (A11) in the Appendix.

Thus, if a significant charge density was present in our patches, the conductance curve in Fig. 9 should approach a non-zero limit at low levels of NaCl. Although it was difficult to measure the channel conductance at very low NaCl concentrations in order to evaluate g_{lim} directly, we argue in the Appendix that, in the presence of surface charges, the tangent to the 'conductance–concentration' curve, drawn from any of its points, will intersect the g-axis at a point whose co-ordinate is always greater than g_{lim}. Denoting this coordinate by g_{int}, we thus have:

$$g_{lim} < g_{int}. \tag{16}$$

Using eqn (A11) for g_{lim}, and expressing the charge density in units of electronic charge per ångström square, and K_M in moles per litre (M), relation (16) becomes:

$$\sigma < \frac{1}{272}\sqrt{\frac{K_M g_{int}}{g_{max} - g_{int}}}, \tag{17}$$

where σ is the charge density, K_M and g_{max} are defined in eqns (14) and (15), respectively, and the meaning of g_{int} is explained above. Drawing the tangent to the curve in Fig. 9 from a point near to the lowest concentration used in the experiments (20 mM), its intersection with the g-axis is about 30 pS. Substituting this value into relation (17), along with those of K_M and g_{max} for Na^+ (see Table 3), the upper limit for σ is found to be about 0·00035 electronic charges per ångström square. This is a fairly small charge density, which would be effectively screened by the ion concentrations used in our experiments, and which suggests either that the charge density at the membrane interfaces is actually small or that its effects do not extend as far as the mouth of the channel.

APPENDIX

A two-site, one-ion model for the glutamate receptor channel. Derivation of the current–voltage equation

A two-site, one-ion model for a channel can exist in five states when two permeant ions are present, as is shown in Fig. 10 for ions Na^+ and X. In this case, five equations can be written to express the fact that, in the steady state, the rate of change for the probabilities of each state must be zero. For example, recalling the definition of the rate constants illustrated in Fig. 10, we have for the probability of state 2, p_2:

$$\frac{dp_2}{dt} = \upsilon'_{Na} p_1 - \mu''_{Na} p_2 + \lambda''_{Na} p_3 - \bar{\lambda}'_{Na} p_2 = 0, \tag{A1}$$

and similar equations can be written for the remaining four states. However, since only four of the five equations thus obtained are independent, one of them must be discarded, and an additional independent equation is required, this being conveniently provided by the normalization of the probabilities

$$\sum_{1=1}^{5} p_1 = 1, \tag{A2}$$

where the subscripts $i (i = 1,2,...5)$ denote the five states of the channel (see Fig. 10).
Solving this system of five equations for p_2, p_3, p_4 and p_5 and substituting in eqns (1) and (2) of the text, one finds explicit expressions for the fluxes, j_{Na} and j_X. The equation for the single-channel current is then obtained from

$$i = e(z_{Na} j_{Na} + z_X j_X). \tag{A3}$$

When Na^+ is sole permeant ion, one finds

$$i = \frac{z_{Na} P_{Na}(1)\left\{a'_{Na}\exp\left(z_{Na}\frac{\phi}{2}\right) - a''_{Na}\exp\left(-z_{Na}\frac{\phi}{2}\right)\right\}}{Q_{Na} + a''_{Na} R_{Na} + a''_{Na} S_{Na}}, \tag{A4}$$

where a'_{Na} and a''_{Na} are the activities of internal and external Na^+, respectively, and where

$$Q_{Na} = \exp\left(z_{Na}(\gamma - \alpha)\frac{\phi}{2}\right) + P_{Na}(4)\exp\left(-z_{Na}(\alpha + \beta)\frac{\phi}{2}\right) + P_{Na}(5)\exp\left(z_{Na}(\beta + \gamma)\frac{\phi}{2}\right),$$

$$R_{Na} = P_{Na}(2)\left\{\exp\left(z_{Na}(\alpha + \gamma)\frac{\phi}{2}\right) P_{Na}(4)\exp\left(z_{Na}(\alpha - \beta)\frac{\phi}{2}\right)\right\} + P_{Na}(3) P_{Na}(4)\exp\left(z_{Na}(\alpha + \beta)\frac{\phi}{2}\right), \tag{A5}$$

$$S_{Na} = P_{Na}(3)\left\{\exp\left(-z_{Na}(\alpha + \gamma)\frac{\phi}{2}\right) + P_{Na}(5)\exp\left(z_{Na}(\beta - \gamma)\frac{\phi}{2}\right)\right\} + P_{Na}(2) P_{Na}(5)\exp\left(-z_{Na}(\beta + \gamma)\frac{\phi}{2}\right).$$

The five quantities, $P_{Na}(1) \ldots P_{Na}(5)$, which appear in eqns (A4) and (A5), are related to the voltage-independent factors of the rate constants by

$$P_{Na}(1) = |e|\bar{\lambda}'_{Na}\frac{\bar{\rho}'_{Na}}{\bar{\mu}''_{Na}}, \quad P_{Na}(2) = \frac{\bar{\rho}'_{Na}}{\bar{\mu}''_{Na}}, \quad P_{Na}(3) = \frac{\bar{\rho}''_{Na}}{\bar{\mu}'_{Na}}, \quad P_{Na}(4) = \frac{\bar{\lambda}''_{Na}}{\bar{\mu}'_{Na}}, \quad P_{Na}(5) = \frac{\bar{\lambda}'_{Na}}{\bar{\mu}''_{Na}}, \tag{A6}$$

$|e|$ being the absolute value of the elementary charge.

If we now denote the numerator and the denominator of eqn (A4) by N_{Na} and D_{Na}, respectively, and if we assume that the fractional distances, α, β and γ $(= 1 - \alpha - \beta)$ are the

same for all ions, the expression for the current in the case of a mixture of two permeant ions, Na^+ and X^+, with X present only in the external solution, is found to be:

$$I = \frac{N_{Na} - z_X(Q_{Na}/Q_X)P_X(1)a''_X \exp\left(-z_X\frac{\phi}{2}\right)}{D_{Na} + (Q_{Na}/Q_X)a''_X S_X}, \tag{A7}$$

where a''_X is the activity of ion X in the external solution, and where Q_X and S_X are defined as in eqn (A5), and $P_X(1)$ as in eqn (A6), provided, of course, that the subscript Na is replaced by X and that z_{Na} is replaced by z_X. Equation (A7) has been used to fit all our data in ion mixtures.

Effects of surface charge density on the channel conductance

The purpose of this section of the Appendix is to derive relation (17) of the Discussion, an inequality which is used there to deduce an upper limit for the surface charge density on the membrane in our preparation.

It is well known that surface charges on the membrane give rise to a surface potential, $\phi(0)$. As a result, the aqueous concentration of ion i at the membrane–solution interface, $C_i(0)$, will be:

$$C_i(0) = C_i e^{-z_i\phi(0)}, \tag{A8}$$

where C_i is the ion concentration in the bulk solution. Assuming: (1) that the Gouy–Chapman theory is valid; (2) that the surface charge effects extend to the channel-mouth area; and (3) that only one monovalent electrolyte is present in solution (e.g. NaCl), eqn (A8) becomes, according to the theory:

$$C_i(0) = C_i + (A/2) + \sqrt{AC_i + A^2/4}\ , \tag{A9}$$

where A is related to the surface charge density σ by:

$$A = (272\sigma)^2, \tag{A10}$$

σ being expressed in electronic charges per square ångström, and C_i in moles per litre (M). Substitution of eqns (A9) and (A10) in eqn (13) yields an expression for the channel conductance as a function of C_i and of the surface charge density. Although, for brevity, we do not give this expression here, two of its features are relevant to our purpose. First, the conductance remains finite even for vanishingly low ion concentrations in the bulk solution. Its limiting value, for $C_i = 0$ and for a uniform and symmetrical charge density, is:

$$g_{lim} = g_{max}\frac{A}{A + K_M}. \tag{A11}$$

Second, the slope of the conductance as a function of C_i decreases as C_i increases. This implies that the straight line tangent to the curve, drawn from any of its points, will intersect the conductance axis at a point whose ordinate, g_{int}, is always greater than g_{lim}. This justifies relation (16) of the Discussion. Finally, substitution of eqns (A10) and (A11) in that relation immediately yields the inequality (17), the result we wished to prove.

REFERENCES

Adams, D. J., Dwyer, T. M. & Hille, B. (1980). The permeability of endplate channels to monovalent and divalent metal cations. *Journal of General Physiology* **75**, 493–510.

Anwyl, R. (1977*a*). Permeability of the post-synaptic membrane of an excitatory glutamate synapse to sodium and potassium. *Journal of Physiology* **273**, 367–388.

Anwyl, R. (1977*b*). The effect of foreign cations, pH and pharmacological agents on the ionic permeability of an excitatory glutamate synapse. *Journal of Physiology* **273**, 389–404.

Ascher, P. & Nowak, L. (1988). The role of divalent cations in the *N*-methyl-D-aspartate responses of mouse central neurones in culture. *Journal of Physiology* **399**, 247–266.

Bregestovski, P. D., Miledi, R. & Parker, I. (1979). Calcium conductance of acetylcholine-induced endplate channels. *Nature* **279**, 638–639.

Butler, J. N. (1968). The thermodynamic activity of calcium ion in sodium chloride–calcium chloride electrolytes. *Biophysical Journal* **8**, 1426–1433.

Collingridge, G. L. & Lester, R. A. J. (1989). Excitatory amino acid receptors in the vertebrate central nervous system. *Pharmacological Reviews* **40**, 143–210.

Cooper, K. E., Gates, P. Y. & Eisenberg, R. S. (1988). Surmounting barriers in ionic channels. *Quarterly Review of Biophysics* **21**, 331–364.

DANI, J. A. & EISENMAN, G. (1987). Monovalent and divalent cation permeation in acetylcholine receptor channels. Ion transport related to structure. *Journal of General Physiology* **89**, 959–983.

DECKER, E. R. & DANI, J. A. (1990). Calcium permeability of the nicotinic acetylcholine receptor: the single-channel calcium influx is significant. *Journal of Neuroscience* **10**, 3413–3420.

DEKIN, M. S. (1983). Permeability changes induced by L-glutamate at the crayfish neuromuscular junction. *Journal of Physiology* **341**, 105–125.

FOSTER, A. C. & FAGG, G. (1984). Acidic amino acid binding sites in mammalian neuronal membranes: their characteristics and relationship to synaptic receptors. *Brain Research Reviews* **7**, 103–164.

GILBERTSON, T. A., SCOBEY, R. & WILSON, M. (1991). Permeation of calcium ions through non-NMDA glutamate channels in retinal bipolar cells. *Science* **251**, 1613–1615.

GOLDMAN, D. E. (1943). Potential, impedance and rectification in membranes. *Journal of General Physiology* **27**, 37–60.

HAMILL, O. P., MARTY, A., NEHER, E., SAKMANN, B. & SIGWORTH, F. J. (1981). Improved patch-clamp techniques for high-resolution current recording from cells and cell-free membrane patches. *Pflügers Archiv* **391**, 85–100.

HILLE, B. (1975). Ionic selectivity of Na and K channels of nerve membranes. In *Membranes; A Series of Advances*, vol. 3, *Lipid Bilayers and Biological Membranes: Dynamic Properties*, ed. EISENMAN, G., pp. 255–323. Mercel Dekker, New York.

HODGKIN, A. L. & KATZ, B. (1949). The effect of sodium ions on the electrical activity of the giant axon of the squid. *Journal of Physiology* **108**, 37–77.

HUANG, L.-Y. M., CATTERALL, W. A. & EHRENSTEIN, G. (1978). Selectivity of cations and nonelectrolytes for acetylcholine-activated channels in cultured muscle cells. *Journal of General Physiology* **71**, 397–410.

IFUNE, C. K. & STEINBACH, J. H. (1991). Voltage-dependent block by magnesium of neuronal nicotinic acetylcholine receptor channels in rat pheochromocytoma cells. *Journal of Physiology* **443**, 683–701.

IINO, M., OZAWA, S. & TSUZUKI, K. (1990). Permeation of calcium through excitatory amino acid receptor channels in cultured rat hippocampal neurones. *Journal of Physiology* **424**, 151–165.

IKEDA, K. (1980). Neuromuscular physiology. In *The Genetics and Biology of Drosophila*, vol. 2d, ed. ASHBURNER, M. & WRIGHT, T. R. F., pp. 369–405. Academic Press, London.

JAN, L. Y. & JAN, Y. N. (1976*a*). Properties of the larval neuromuscular junction in *Drosophila melanogaster*. *Journal of Physiology* **262**, 189–214.

JAN, L. Y. & JAN, Y. N. (1976*b*). L-Glutamate as an excitatory transmitter at the *Drosophila* larval neuromuscular junction. *Journal of Physiology* **262**, 215–236.

KIDOKORO, Y. & CHANG, H. (1991). Kinetic properties of glutamate receptor channels in embryonic *Drosophila* myotubes in culture. *Biomedical Research* **12**, suppl., 73–76.

LASSIGNAL, N. L. & MARTIN, A. R. (1977). Effect of acetylcholine on postjunctional membrane permeability in eel electroplaque. *Journal of General Physiology* **70**, 23–36.

LÄUGER, P. (1973). Ion transport through pores: a rate theory analysis. *Biochimica et Biophysica Acta* **311**, 423–441.

LEWIS, C. A. (1979). Ion-concentration dependence of the reversal potential and the single channel conductance of ion channels at the frog neuromuscular junction. *Journal of Physiology* **286**, 417–445.

LINDER, T. M. & QUASTEL, D. M. J. (1978). A voltage-clamp study of the permeability change induced by quanta of transmitter at the mouse end-plate. *Journal of Physiology* **281**, 535–556.

MCLAUGHLIN, S. (1989). The electrostatic properties of membranes. *Annual Review of Biophysics and Biophysical Chemistry* **18**, 113–136.

MAGLEBY, K. L. & WEINSTOCK, M. M. (1980). Nickel and calcium ions modify the characteristics of the acetylcholine receptor–channel complex at the frog neuromuscular junction. *Journal of Physiology* **299**, 203–218.

MARCHAIS, D. & MARTY, A. (1979). Interaction of permeant ions with channels activated by acetylcholine in *Aplysia* neurones. *Journal of Physiology* **297**, 9–45.

MAYER, M. & WESTBROOK, G. L. (1987*a*). The physiology of excitatory amino acids in the vertebrate central nervous system. *Progress in Neurobiology* **28**, 197–276.

MAYER, M. & WESTBROOK, G. L. (1987*b*). Permeation and block of *N*-methyl-D-aspartic acid receptor channels by divalent cations in mouse cultured central neurones. *Journal of Physiology* **394**, 501–527.

MAYER, M. L., WESTBROOK, G. L. & GUTHRIE, P. B. (1984). Voltage-dependent block by Mg^{2+} of NMDA responses in spinal cord neurones. *Nature* **309**, 261–263.

MONAGHAN, D. T., BRIDGES, R. J. & COTMAN, C. W. (1989). The excitatory amino acid receptors: their classes, pharmacology, and distinct properties in the function of the central nervous system. *Annual Review of Pharmacology and Toxicology* **29**, 365–402.

NEUHAUS, R. & CACHELIN, A. B. (1990). Changes in the conductance of the neuronal nicotinic acetylcholine receptor channel induced by magnesium. *Proceedings of the Royal Society* B **241**, 78–84.

NOWAK, L., BREGESTOVSKI, P., ASCHER, P., HERBET, A. & PROCHIANTZ, A. (1984). Magnesium gates glutamate-activated channels in mouse central neurones. *Nature* **307**, 462–465.

PRESS, W. H., FLANNERY, B. P., TEUKOLSKY, S. A. & VETTERLING, W. T. (1988). *Numerical Recipes in C*. Cambridge University Press, Cambridge, New York.

ROBINSON, R. A. & STOKES, R. H. (1965). *Electrolyte Solutions*, 2nd edn, revised. Butterworths, London.

ROTHMAN, S. M. & OLNEY, J. W. (1987). Excitotoxicity and the NMDA receptor. *Trends in Neurosciences* **10**, 299–302.

SANCHEZ, J. A., DANI, J. A., SIEMEN, D. & HILLE, B. (1986). Slow permeation of organic cations in acetylcholine receptor channels. *Journal of General Physiology* **87**, 985–1001.

SCHUSTER, C. M., ULTSCH, A., SCHLOSS, P., COX, J. A., SCHMITT, B. & BETZ, H. (1991). Molecular cloning of an invertebrate glutamate receptor subunit expressed in *Drosophila* muscle. *Science* **254**, 112–114.

SHATKAY, A. (1968). Individual activity of calcium ions in pure solutions of $CaCl_2$ and in mixtures. *Biophysical Journal* **8**, 912–919.

TAKEUCHI, A. & TAKEUCHI, N. (1964). The effect on crayfish muscle of iontophoretically applied glutamate. *Journal of Physiology* **170**, 296–317.

USHERWOOD, P. N. R. & CULL-CANDY, S. G. (1975). Pharmacology of somatic nerve–muscle synapses. In *Insect Muscle*, ed. USHERWOOD, P. N. R., pp. 207–280. Academic Press, London.

WEAST, R. C., ASTLE, M. J. & BEYER, W. H. (1985). *CRC Handbook of Chemistry and Physics*. CRC Press, Boca Raton, FL, USA.

Acknowledgements

We thank Drs K. Ikeda, P. Salvaterra, I. Hayashi, and L. Byerly for helpful advice on the methods for culturing embryonic *Drosophila* muscle. This study was supported by NIH grant (R01NS23753) to Y.K.

Author's present address

H. Chang: University of Tokyo School of Medicine, 3-28-6 Mejirodai, Bunkyo-ku, Tokyo 112, Japan.

Received 29 October 1992; revised 12 July 1993; accepted 19 August 1993.